

Results on spin-dependent WIMP-nucleon interaction from first data of PandaX-II experiment

Changbo Fu,¹ Xiangyi Cui,¹ Xiaopeng Zhou,² Xun Chen,¹ Yunhua Chen,³ Deqing Fang,⁴ Karl Giboni,¹ Franco Giuliani,^{1,5} Ke Han,¹ Xingtao Huang,⁶ Xiangdong Ji,^{1,5,7,8,*} Yonglin Ju,⁹ Siao Lei,¹ Shaoli Li,¹ Huaxuan Liu,⁹ Jianglai Liu,¹ Yugang Ma,⁴ Yajun Mao,² Xiangxiang Ren,¹ Andi Tan,⁷ Hongwei Wang,⁴ Jiming Wang,³ Meng Wang,⁶ Qihong Wang,⁴ Siguang Wang,² Xuming Wang,¹ Zhou Wang,⁹ Shiyong Wu,³ Mengjiao Xiao,^{7,5} Pengwei Xie,¹ Binbin Yan,^{6,†} Yong Yang,^{1,‡} Jianfeng Yue,³ Hongguang Zhang,¹ Tao Zhang,¹ Li Zhao,¹ and Ning Zhou^{1,10}

(PandaX-II Collaboration)

¹*INPAC and Department of Physics and Astronomy, Shanghai Jiao Tong University, Shanghai Laboratory for Particle Physics and Cosmology, Shanghai 200240, China*

²*School of Physics, Peking University, Beijing 100871, China*

³*Yalong River Hydropower Development Company, Ltd., 288 Shuanglin Road, Chengdu 610051, China*

⁴*Shanghai Institute of Applied Physics, Chinese Academy of Sciences, 201800, Shanghai, China*

⁵*Center of High Energy Physics, Peking University, Beijing 100871, China*

⁶*School of Physics and Key Laboratory of Particle Physics and Particle Irradiation (MOE), Shandong University, Jinan 250100, China*

⁷*Department of Physics, University of Maryland, College Park, Maryland 20742, USA*

⁸*T. D. Lee Institute, Shanghai 200240, China*

⁹*School of Mechanical Engineering, Shanghai Jiao Tong University, Shanghai 200240, China*

¹⁰*Department of Physics, Tsinghua University, Beijing 100084, China*

(Dated: January 10, 2017)

New constraints are presented on the spin-dependent WIMP-nucleon interaction from the PandaX-II experiment, using a data set corresponding to a total exposure of 3.3×10^4 kg-days. Assuming a standard axial-vector spin-dependent WIMP interaction with ^{129}Xe and ^{131}Xe nuclei, the most stringent upper limits on WIMP-neutron cross sections for WIMPs with masses above $10 \text{ GeV}/c^2$ are set in all dark matter direct detection experiments. The minimum upper limit of $4.1 \times 10^{-41} \text{ cm}^2$ at 90% confidence level is obtained for a WIMP mass of $40 \text{ GeV}/c^2$. This represents more than a factor of two improvement on the best available limits at this and higher masses. These improved cross-section limits provide more stringent constraints on the effective WIMP-proton and WIMP-neutron couplings.

The existence of dark matter (DM) in the Universe has been established by numerous pieces of astronomical and cosmological evidence. These range from the dynamics, gravitational lensing, and clustering of galaxies to the necessity of DM to explain the power spectrum of the cosmic microwave background and the formation of cosmological structures. However, the particle nature of DM still remains elusive. Weakly interacting massive particles (WIMPs), a class of hypothetical particles predicted by many extensions of the Standard Model of particle physics, are promising candidates for DM. Generic WIMP production and annihilation rates in the early universe would lead to a freeze-out WIMP density which could explain the observed DM relic density (the so-called “WIMP miracle” [1]). The detection of WIMP signals is the goal of many past, ongoing and future experiments, including direct detection experiments, indirect detection experiments, and experiments at colliders.

The PandaX project consists of a series of xenon-based experiments, located at the China JinPing underground

Laboratory (CJPL). The first two experiments, PandaX-I and PandaX-II, use xenon as a target to search for WIMPs. The third experiment PandaX-III [2], which is being prepared, will search for neutrinoless double beta decay of ^{136}Xe . PandaX-I, with a 120-kg xenon target, was completed in 2014. PandaX-II, with a half-ton xenon target, has been running since the end of 2015. Both the PandaX-I and PandaX-II experiments use a dual-phase xenon time projection chamber technique. With this technique, both the prompt scintillation photons (S1) produced in liquid xenon and the delayed electroluminescence photons (S2) produced in gaseous xenon for each physical event can be measured. This leads to powerful background suppression and signal-background discrimination. More detailed descriptions of the PandaX-I and PandaX-II experiments can be found in Refs. [3–6].

The PandaX-II collaboration has recently reported WIMP search results [6] using the first 98.7 days of data. This data set corresponds to a total exposure of 3.3×10^4 kg-days. No excess of events was observed above the background, and WIMP-nucleon cross-section upper limits were set assuming a spin-independent (SI) WIMP-nucleon interaction. The best upper limit of $2.5 \times 10^{-46} \text{ cm}^2$ for a WIMP mass of $40 \text{ GeV}/c^2$ was obtained. In this paper we consider an axial-vector,

* Spokesperson: xdj@sjtu.edu.cn

† Corresponding author: bbyan@hepg.sdu.edu.cn

‡ Corresponding author: yong.yang@sjtu.edu.cn

spin-dependent (SD) interaction, which is well motivated if WIMPs have spin. An example of this would be the lightest neutralino in the supersymmetric theories, which offers one of the most promising DM explanations. Xenon-based experiments, such as PandaX, XENON and LUX, are sensitive to this interaction because xenon contains a significant fraction of isotopes with non-zero spin. LUX experiment [7], with a total exposure of 1.4×10^4 kg-days, pushed down the SD WIMP-neutron and WIMP-proton cross-section limits to 9.4×10^{-41} cm² and 2.9×10^{-39} cm², respectively, at a WIMP mass of 33 GeV/c². XENON100 experiment [8] recently updated their SD results with a total exposure of 1.8×10^4 kg-days, obtaining slightly less stringent limits.

We use the same data set and identical event reconstruction and selections as in Ref. [6]. Compared to [6], the data and expected background after selections remain unchanged. Below we describe the WIMP-nucleus recoil rate calculation for the SD WIMP-nucleon interaction, which will be needed to calculate the S1 and S2 signal distributions and the final WIMP-nucleon cross-section upper limits.

The nuclear recoil energy due to a WIMP with mass m scattering elastically from a nucleus with mass M is $E = (\mu^2 v^2 / M)(1 - \cos \theta)$, where μ is the reduced mass, v is the speed of the WIMP relative to the nucleus, and θ is the scattering angle in the center of mass frame. The differential event rate with respect to recoil energy, in units of counts/keV/day/kg of xenon, can be written as [9]

$$\frac{dR}{dE} = \frac{\sigma^A(q)}{2m\mu^2} \rho \eta(E, t), \quad (1)$$

where $q = \sqrt{2ME}$ is the nuclear recoil momentum, $\sigma^A(q)$ is the WIMP-nucleus cross section, ρ is the local WIMP density, and $\eta(E, t)$ is the mean inverse speed of the time-dependent WIMP velocity distribution relative to the detector. The most frequently used distribution for the WIMP speed relative to the Milky way halo is a Maxwellian distribution with the most probable value at $v_0 = 220$ km/s, and which is truncated at the galactic escape velocity $v_{\text{esc}} = 544$ km/s. The calculation of Eq. 1 follows the procedure in Ref. [9].

To report results for SD interactions, a common practice is to consider the two limiting cases in which the WIMPs couple only to protons or to neutrons. This practice is also consistent with the fact that, due to the cancellation between spins of nucleon pairs, for odd-A nuclei, $\sigma^A(q)$ is dominated by either contributions from the unpaired proton (odd Z) or neutron (even Z). The intermediate cases can be treated by following the methods in Ref. [10]. In the two limiting cases, the SD WIMP-nucleus cross section can then be written as

$$\sigma_{p,n}^A(q) = \frac{4\pi\mu^2 S_{p,n}(q)}{3(2J+1)\mu_{p,n}^2} \sigma_{p,n}, \quad (2)$$

where $\mu_{p,n}$ is the WIMP-proton or WIMP-neutron reduced mass, $\sigma_{p,n}$ is the WIMP-proton or WIMP-neutron

cross section and J is the total angular momentum of the nucleus. Due to the above mentioned spin pairing effects, the main Xe isotopes sensitive to SD interactions are ^{129}Xe ($J=1/2$) and ^{131}Xe ($J=3/2$). The corresponding abundance in natural xenon is 26.4% and 21.2%, respectively.

In Eq. 2 $S_{p,n}(q)$ is the spin structure factor for proton-only or neutron-only coupling, obtained from nuclear shell model calculations. In this paper we use the most recent calculation by Klos *et al.* [11] based on chiral effective field theory at the one-body level, including the leading long-range two-body currents. With this calculation, the ground states and the ordering of the excited states of ^{129}Xe and ^{131}Xe are very well described. This calculation was also used in recent SD results from LUX [7] and XENON100 [8]. Alternative calculations by Ressel and Dean [12] and by Toivanen *et al.* [13] generally do not agree with each other nor with that by Klos *et al.* [11]. A comparison of these calculations can be found in Ref. [14].

For illustration, we compare structure factors using the calculation from Ref. [11] as a function of nuclear recoil energy for proton-only and neutron-only couplings. This is shown in Fig. 1. For both ^{129}Xe and ^{131}Xe , the neutron-only structure factor is much larger than proton-only, since the total nuclear spin is dominated by the unpaired neutron. It is worth noting (as in Ref. [11]) that “neutron/proton-only” is simply a notation for convenience. When two-body currents are included, neutrons can contribute to the proton-only coupling. This in fact significantly enhances the proton-only while slightly reducing the neutron-only structure factor.

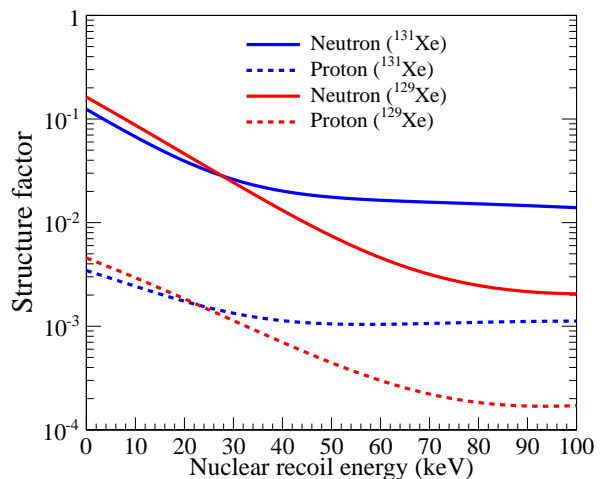


FIG. 1: Structure factors as a function of nuclear recoil energy for neutron-only (plain) and proton-only (dashed) couplings for ^{129}Xe (red) and ^{131}Xe (blue), using the calculations from Ref. [11].

Fig. 2 shows the calculated recoil-energy distributions without detector effects for two WIMP masses 40 GeV/c² and 400 GeV/c², for neutron-only and proton-only cou-

plings. Here the WIMP-neutron and WIMP-proton cross sections are assumed to be $\sigma_n = 10^{-40} \text{ cm}^2$ and $\sigma_p = 3 \times 10^{-39} \text{ cm}^2$, respectively. This allows the two cases be compared directly. The recoil-energy distribution for proton-only coupling is harder than neutron-only, since the proton-only structure factor decreases more slowly at high recoil energies compared to the neutron-only.

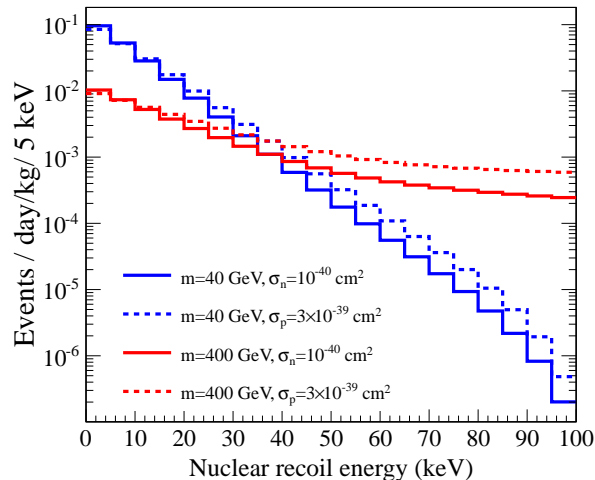


FIG. 2: Nuclear recoil-energy distributions without detector effects for two WIMP mass points 40 GeV/c² (blue) and 400 GeV/c² (red), for neutron-only (plain) and proton-only (dashed) couplings. Here we use dR/dE calculations from Ref. [9] and structure factor calculations from Ref. [11]. The WIMP-neutron and WIMP-proton cross sections are assumed to be $\sigma_n = 10^{-40} \text{ cm}^2$ and $\sigma_p = 3 \times 10^{-39} \text{ cm}^2$, respectively, for visual clarity.

As in Ref. [6], the data set is divided into 15 time bins to take into account the temporal change of detector parameters and background rates. For each time bin, we simulate S1 and S2 signal distributions from the obtained WIMP nuclear recoil-energy distributions using the NEST model [15]. We apply the same S1 and S2 selections as in Ref. [6], requiring an S1 in the range of 3 photoelectrons (PE) and 45 PE and an S2 in the range of 100 PE (uncorrected) and 10000 PE. Fig. 3 shows the final detection efficiency per WIMP-xenon interaction (weighted average of 15 time bins) as a function of the WIMP mass for the neutron-only and proton-only SD interactions. The efficiency for SI interaction is also included for comparison. Here, all measured efficiencies for data quality, S1 and S2 selections, as well as the additional boosted-decision-tree selection for suppressing accidental background have been taken into account. For SD interaction, the efficiency increases from approximately 2% ($m = 10 \text{ GeV}/c^2$) to approximately 45% at high masses. The difference between proton-only and neutron-only couplings is due to the difference of the recoil-energy distributions (Fig. 2) and the dependence

of the efficiency on recoil energy (Fig. 2 in Ref. [6]).

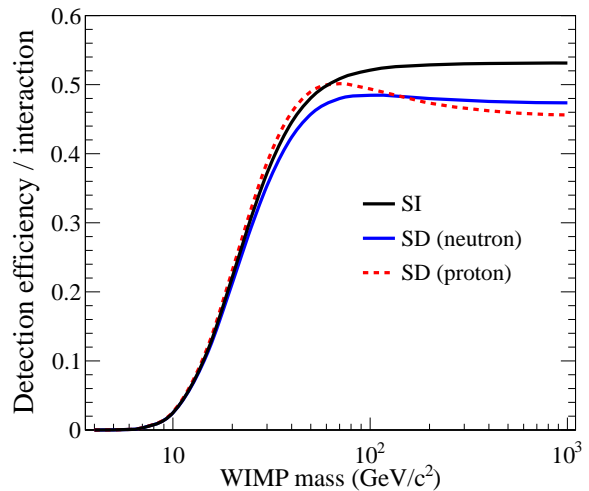


FIG. 3: Detection efficiency per interaction as a function of the WIMP mass for neutron-only (blue) and proton-only (red) SD interactions. Efficiency for SI interaction (black) is also plotted for comparison.

The upper limits for the SD WIMP-nucleon cross sections are calculated with the same procedure as in Ref. [6]. Test statistics based on profile likelihood ratio [23, 24] were constructed over grids of WIMP mass and cross section. Then, the 90% confidence level (CL) upper limits of cross sections were calculated using the CL_s approach [25, 26]. The results are shown in Fig. 4, with recent results from other experiments overlaid. The upper limits presented lie within the $\pm 1\sigma$ sensitivity band. The lowest cross-section limit obtained is $4.1 \times 10^{-41} \text{ cm}^2$ ($1.2 \times 10^{-39} \text{ cm}^2$) for WIMP-neutron (WIMP-proton) elastic scattering at a WIMP mass of 40 GeV/c². For neutron-only coupling, the lowest exclusion limits for WIMP above 10 GeV/c² in direct detection experiments are obtained. Under model assumptions, results from DM searches at colliders can also be interpreted as the WIMP-nucleon cross-section limits. For example, mono-jet search results from CMS [16] and ATLAS [18] have been interpreted in the framework of the so-called “simplified” DM model [17, 27, 28] which includes four parameters: the DM mass, the mediator mass, the coupling of the mediator to DM particles (g_{DM}) and the coupling of the mediator to quarks (g_q). Four coupling scenarios $g_q = g_{\text{DM}} = 0.25, 0.5, 1.0$ and 1.45 have been considered in Ref. [17] for interpreting the CMS results. The ATLAS collaboration reported the limits for the couplings $g_q = 0.25$ and $g_{\text{DM}} = 1$. In Fig. 4 we include the limits obtained from the smallest and the largest couplings from CMS and the limits from ATLAS. These limits are particularly strong for low mass WIMPs, but one should note the strong model dependence. Our SD WIMP-proton cross-section limits are much weaker than the WIMP-neutron ones due to the even number

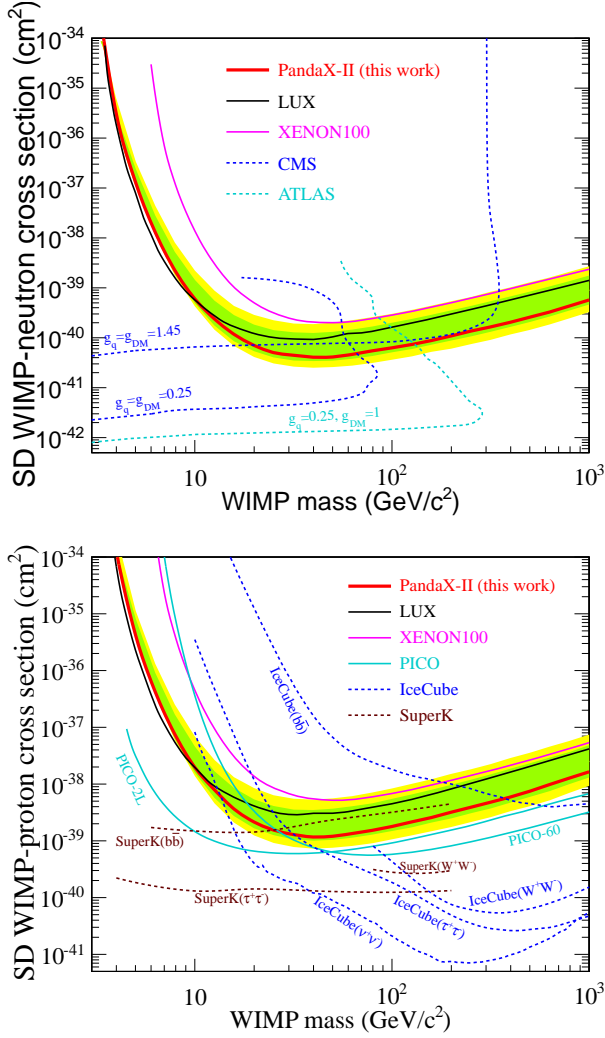


FIG. 4: PandaX-II 90% CL upper limits for the SD WIMP-neutron (top) and WIMP-proton (bottom) cross sections. Selected recent world results are plotted for comparison: LUX [7], XENON100 [8], CMS mono-jet [16, 17], ATLAS mono-jet [18], PICO-2L [19], PICO-60 [20], IceCube [21] and Super-K [22]. The 1 and 2- σ sensitivity bands are shown in green and yellow, respectively.

of protons and the unpaired neutron in ^{129}Xe and ^{131}Xe nuclei. PICO experiments [19, 20], on the other hand, utilizing ^{19}F nucleus which contains an unpaired proton, produced so far the most stringent constraints on the SD WIMP-proton cross sections in all direct search experiments. Indirect search experiments, IceCube [21] and Super-K [22], can produce more stringent limits, depending on WIMP masses and annihilation channels.

The WIMP-neutron and WIMP-proton cross-section upper limits can be used to constrain the effective WIMP couplings to neutrons and protons, a_n and a_p , simultaneously. For a given WIMP mass, the allowed region in

the a_p - a_n plane is derived from [29, 30]

$$\sum_A \left(\frac{a_p}{\sqrt{\sigma_p^{\text{lim}(A)}}} \pm \frac{a_n}{\sqrt{\sigma_n^{\text{lim}(A)}}} \right)^2 \leq \frac{\pi}{24G_F^2 \mu_p^2}, \quad (3)$$

where $\sigma_{p,n}^{\text{lim}(A)}$ are the upper limits of the WIMP-proton and WIMP-neutron cross sections for the isotope with mass number A . Fig 5 shows the allowed region in the a_p - a_n plane, together with results from LUX, PICO, and CDMS experiments (all calculated in Ref. [7]) for two WIMP masses (50 and 1000 GeV/c^2). This shows our improvement over previous results, as well as the complementarity between experiments with different detection mediums.

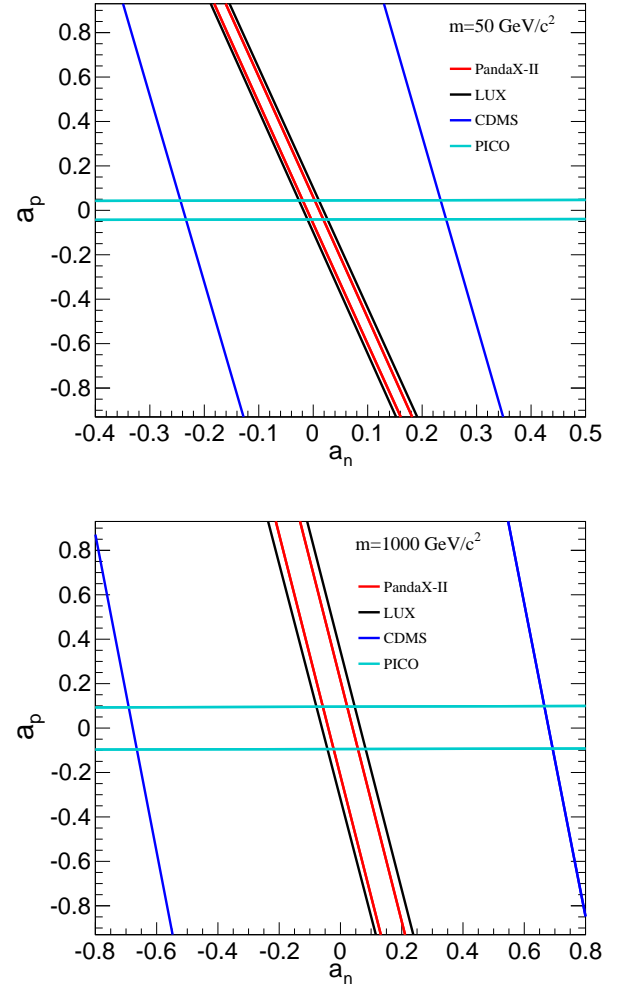


FIG. 5: PandaX-II constraints on the effective WIMP-proton and WIMP-neutron couplings, a_p and a_n , for two WIMP masses (50 and 1000 GeV/c^2). Also shown are results from LUX, PICO and CDMS experiments (all from Ref. [7]).

In conclusion, the 90% CL upper limits of the SD WIMP-nucleon cross section using recently released data

of the PandaX-II experiment with a total exposure of 3.3×10^4 kg-days have been presented. For WIMPs with masses above $10 \text{ GeV}/c^2$, the most stringent upper limits to date on the SD WIMP-neutron cross sections in all direct DM search experiments are set, with a lowest excluded value of $4.1 \times 10^{-41} \text{ cm}^2$ at a WIMP mass of $40 \text{ GeV}/c^2$. This result is complementary to the results obtained from WIMP searches performed at the LHC, which can produce strong limits particularly for low mass WIMPs, depending on the models and assumptions. For high mass WIMPs, the constraints on the effective WIMP-proton and WIMP-neutron couplings have also been improved over previous results from direct DM search experiments. These constraints are complementary to experiments (such as PICO), which are more sensitive to WIMP-proton than WIMP-neutron coupling.

ACKNOWLEDGMENTS

This project has been supported by a 985-III grant from Shanghai Jiao Tong University, grants from the National Science Foundation of China (Nos. 11435008, 11455001, 11505112 and 11525522), a grant from the Office of Science and Technology in Shanghai Municipal Government (No. 11DZ2260700), and a grant from the Ministry of Science and Technology of China (No. 2016YFA0400301). This work is supported in part by the Chinese Academy of Sciences Center for Excellence in Particle Physics (CCEPP), the Key Laboratory for Particle Physics, Astrophysics and Cosmology, Ministry of Education, and Shanghai Key Laboratory for Particle Physics and Cosmology (SKLPPC). The project is also sponsored by Shandong University, Peking University, and the University of Maryland. We thank C. Hall for helping with the specifics of tritium calibration. We thank P. Klos *et al.* for providing their structure factor calculations. We also thank the CJPL administration and the Yalong River Hydropower Development Company Ltd for indispensable logistics and other support. Finally, we thank the Hong Kong Hongwen Foundation for financial support.

-
- [1] G. Jungman, M. Kamionkowski, and K. Griest, Phys. Rept. **267**, 195 (1996), arXiv:hep-ph/9506380 [hep-ph].
 - [2] X. Chen *et al.*, (2016), arXiv:1610.08883 [physics.ins-det].
 - [3] M. Xiao *et al.* (PandaX), Sci. China Phys. Mech. Astron. **57**, 2024 (2014), arXiv:1408.5114 [hep-ex].
 - [4] X. Xiao *et al.* (PandaX), Phys. Rev. **D92**, 052004 (2015), arXiv:1505.00771 [hep-ex].
 - [5] A. Tan *et al.* (PandaX), Phys. Rev. **D93**, 122009 (2016), arXiv:1602.06563 [hep-ex].
 - [6] A. Tan *et al.* (PandaX-II), Phys. Rev. Lett. **117**, 121303 (2016), arXiv:1607.07400 [hep-ex].
 - [7] D. S. Akerib *et al.* (LUX), Phys. Rev. Lett. **116**, 161302 (2016), arXiv:1602.03489 [hep-ex].
 - [8] E. Aprile *et al.* (XENON100), (2016), arXiv:1609.06154 [astro-ph.CO].
 - [9] C. Savage, G. Gelmini, P. Gondolo, and K. Freese, JCAP **0904**, 010 (2009), arXiv:0808.3607 [astro-ph].
 - [10] F. Giuliani, Phys. Rev. Lett. **93**, 161301 (2004), arXiv:hep-ph/0404010 [hep-ph].
 - [11] P. Klos, J. Menéndez, D. Gazit, and A. Schwenk, Phys. Rev. **D88**, 083516 (2013), [Erratum: Phys. Rev. **D89**, no. 2, 029901 (2014)], arXiv:1304.7684 [nucl-th].
 - [12] M. T. Ressell and D. J. Dean, Phys. Rev. **C56**, 535 (1997), arXiv:hep-ph/9702290 [hep-ph].
 - [13] P. Toivanen, M. Kortelainen, J. Suhonen, and J. Toivanen, Phys. Rev. C **79**, 044302 (2009).
 - [14] E. Aprile *et al.* (XENON100), Phys. Rev. Lett. **111**, 021301 (2013), arXiv:1301.6620 [astro-ph.CO].
 - [15] B. Lenardo, K. Kazkaz, M. Szydagis, and M. Tripathi, IEEE Trans. Nucl. Sci. **62**, 3387 (2015), arXiv:1412.4417 [astro-ph.IM].
 - [16] V. Khachatryan *et al.* (CMS), Eur. Phys. J. **C75**, 235 (2015), arXiv:1408.3583 [hep-ex].
 - [17] S. A. Malik *et al.*, Phys. Dark Univ. **9-10**, 51 (2015), arXiv:1409.4075 [hep-ex].
 - [18] M. Aaboud *et al.* (ATLAS), Phys. Rev. **D94**, 032005 (2016), arXiv:1604.07773 [hep-ex].
 - [19] C. Amole *et al.* (PICO), Phys. Rev. **D93**, 061101 (2016), arXiv:1601.03729 [astro-ph.CO].
 - [20] C. Amole *et al.* (PICO), Phys. Rev. **D93**, 052014 (2016), arXiv:1510.07754 [hep-ex].
 - [21] M. G. Aartsen *et al.* (IceCube), JCAP **1604**, 022 (2016), arXiv:1601.00653 [hep-ph].
 - [22] K. Choi *et al.* (Super-Kamiokande Collaboration), Phys. Rev. Lett. **114**, 141301 (2015).
 - [23] G. Cowan, K. Cranmer, E. Gross, and O. Vitells, Eur. Phys. J. **C71**, 1554 (2011), [Erratum: Eur. Phys. J. **C73**, 2501 (2013)], arXiv:1007.1727 [physics.data-an].
 - [24] E. Aprile *et al.* (XENON100), Phys. Rev. **D84**, 052003 (2011), arXiv:1103.0303 [hep-ex].
 - [25] A. L. Read, J. Phys. **G28**, 2693 (2002).
 - [26] T. Junk, Nucl. Instrum. Meth. **A434**, 435 (1999), arXiv:9902006 [hep-ex].
 - [27] O. Buchmueller, M. J. Dolan, S. A. Malik, and C. McCabe, JHEP **01**, 037 (2015), arXiv:1407.8257 [hep-ph].
 - [28] D. Abercrombie *et al.*, (2015), arXiv:1507.00966 [hep-ex].
 - [29] D. R. Tovey, R. J. Gaitskell, P. Gondolo, Y. A. Ramachers, and L. Roszkowski, Phys. Lett. **B488**, 17 (2000), arXiv:hep-ph/0005041 [hep-ph].
 - [30] F. Giuliani and T. A. Girard, Phys. Rev. **D71**, 123503 (2005), arXiv:hep-ph/0502232 [hep-ph].